Physics of Fluids ARTICLE pubs.aip.org/aip/pof

Resonant effects of long-period ship-induced waves near shallow coasts

Cite as: Phys. Fluids **36**, 107126 (2024); doi: 10.1063/5.0222727
Submitted: 10 June 2024 · Accepted: 7 September 2024 ·
Published Online: 7 October 2024

View Online Export Citation CrossMark

León-Carlos Dempwolff,[1,a] Christian Windt,[1,b] Gregor Melling,[2,c] Ingrid Holzwarth,[2,d] Hans Bihs,[3,e] and Nils Goseberg[1,f]

AFFILIATIONS

[1]Technische Universität Braunschweig, Leichtweiß-Institute for Hydraulic Engineering and Water Resources, 38106 Braunschweig, Germany
[2]German Federal Waterways Engineering and Research Institute (BAW), 22559 Hamburg, Germany
[3]Norwegian University of Science and Technology (NTNU), Department of Civil and Environmental Engineering, 7491 Trondheim, Norway

[a]**Author to whom correspondence should be addressed:** l.dempwolff@tu-braunschweig.de
[b]**Electronic mail:** c.windt@tu-braunschweig.de
[c]**Electronic mail:** gregor.melling@baw.de
[d]**Electronic mail:** ingrid.holzwarth@baw.de
[e]**Electronic mail:** hans.bihs@ntnu.no
[f]**Also at**: Coastal Research Center (FZK), Joint Research Facility of Leibniz University Hannover and Technische Universität Braunschweig, 30419 Hannover, Germany. **Electronic mail:** n.goseberg@tu-braunschweig.de

ABSTRACT

This work analyzes the propagation properties of long-period ship-induced waves of vessels in confined waterways that are surrounded by wide and shallow water bodies using numerical simulations. Previous measurements indicated that, in the presence of shallow water surroundings, the drawdown being part of the long-period wave system can travel in the form of depression waves over several ship lengths distance [Parnell *et al.*, "Ship-induced solitary Riemann waves of depression in Venice Lagoon," Phys. Lett. A **379**, 555–559 (2015); Scarpa *et al.*, "The effects of ship wakes in the Venice Lagoon and implications for the sustainability of shipping in coastal waters," Sci. Rep. **9**, 19014 (2019)]. The exact conditions leading to these unexpectedly large propagation distances could to date not be clarified [Parnell *et al.*, "Depression Waves Generated by Large Ships in the Venice Lagoon," J. Coastal Res. **75**, 907–911 (2016)]. In this work, evidence from numerical simulations is presented, indicating that the far-field propagation properties are governed by the wave speed of the shallow water surroundings. In case the ship speed is larger than the surrounding wave speed (supercritical conditions), a free wave is continuously generated traveling over the shallow water with only minimal height decay. In the simulations, depression waves can travel over a distance of three ship-lengths with a height reduction below 10% in the supercritical regime, as compared to 80% height reduction in the sub-critical regime. In a one-dimensional environment, this agreement of free and forced wave speed is known as Proudman resonance.

I. INTRODUCTION

A. Motivation

Ship hulls in motion generate complex superimposed wave systems consisting of several components, such as the long-period primary wave system, the short-period secondary wave system, and precursor solitons.[4,5] The long-period primary wave system is a result of the hydrodynamic flow field around the ship hull.[6] It consists of a bow wave above the still water level, a water level depression or drawdown along the ship hull, and a stern wave with positive elevation above the still water level. The amplitudes of these wave components are assumed to be highest near the hull, decaying with greater distance to the ship's sailing line.[6] The amplitude of this wave system amplifies in settings, where the vessel's cross-sectional area is large in relation to the waterway cross section;[5] this ratio is often termed the blockage factor.

Ship-induced primary waves were, therefore, often examined with a focus on inland waterways; however, increasing vessel dimensions in past decades have led to notable primary waves in coastal and estuarine waterways as well.[7–10] To enable navigation in these waterways, the ships usually travel in artificially deepened fairways, which are surrounded by relatively shallow water.[1,2,7,11,12]

If such navigation conditions are present, the ship-induced drawdown was found to travel in the form of long-living depression waves, such that a surprisingly large wave height was measured in several ship-length distance to the fairway.[1,7,12] In particular, for the Venice Lagoon, it is well documented that at a measurement site on the Malamocco–Marghera industrial channel, the height of this depression wave is not necessarily correlated with the ship speed and blockage factors, as often considered in semi-empirical equations as reviewed by Almström and Larson.[8] In contrast, moderately sized ships are also reported generating depression waves of significant amplitude.[1,2,7] The wave deformation resulting in a steep rear front could be described as the result of highly nonlinear deformation following Riemann wave theory,[1,13] yet the reason for the long travel distances could not be attributed to justifiable underlying physical processes.[2,3] It is suspected that the long propagation distance is the result of wave deformation in shallow water particular to long-period forced waves; however, the mechanism is not understood to date.[2] Furthermore, measurements from the Lido and Giudecca channels at the Venice lagoon traveled by cruise ships revealed that the depression wave heights were much smaller than expected from the experience at the Malamocco–Marghera channel, even though the vessels had similar blockage factors.[3] In addition, field measurements indicate that the propagation direction of the primary wave system deviates from the ship's motion direction.[2,7] Similar to the unexpected propagation distances, the propagation direction could not be described by existing theoretical frameworks, hence requiring further research on the underlying drivers. These observations motivate this work, triggering further research into understanding the propagation mechanisms by testing ships surrounded by wide and shallow areas.[3]

The need to understand these far-field propagation properties of ship-induced depression waves is nowadays enhanced, as these long-period ship wave components are a serious concern for the design of many confined waterways worldwide.[5] Damage to the built environment is frequently reported, stipulating costly repair work,[12,14–18] as well as adverse impact on the natural environment[9,19,20] and modification of the morphodynamic activity of waterways;[21–23] there even is a human fatality documented.[24] It is widely acknowledged that the challenges in the prediction of long-period ship-induced waves for design purposes reside in the complex interaction effects between features of the bathymetry, such as varying embankment geometries, and the long-period forced waves. Some of the unexpectedly high loads can be attributed to shallow water deformation, such as shoaling.[12,25] Yet, the underlying causes and effects are not sufficiently well described in detail yet but rather serve as a reason to develop sophisticated numerical models.[26]

To that end, in Sec. I B, the different interaction effects of long-period bound waves with the surrounding bathymetry are first outlined in the form of a literature review, aiming to distill the remaining lack of knowledge in shallow water effects of long-period depression ship waves. Several authors have reported on the analogies between ship-induced waves and landslide tsunamis[27] or meteotsunamis.[1,28,29] Therefore, this literature review not only is not limited to the deformation of ship-induced waves but also includes literature on landslides and meteotsunamis, to look at analogous wave physics' effects and potentially facilitate a transfer onto ship-induced waves.

B. Shallow water effects of long-period bound waves

Four different phenomena are reported to govern the interaction of long-period bound waves with a given bathymetry. These are free waves generated at a sudden and pronounced topographic change normal to the propagation direction,[28,30,31] edge wave generation at inclined coasts (Greenspan resonance),[23] and the briefly mentioned nonlinear depression wave deformation following the theory of Riemann waves.[1,13] A fourth phenomenon occurring when a forced wave travels with shallow water wave celerity is the Proudman resonance, known to cause amplification of wave heights if bound wave and free wave speed matches.[32] An illustration of these different phenomena is provided in Fig. 1.

The generation of free waves generated when a ship travels over a step oriented normal to the sailing line has first been reported by Grue.[30] In the Oslo fjord, large conventional ferries (as compared to fast ferries) travel over abrupt changes in the water depth from 80 m to only 11 m along the sailing line in the most extreme cases. At the coast, wave heights up to 1.4 m at a period of 30–60 s are measured ahead of the ships.[30] A generation mechanism is derived based on a vertical flow component induced at the depth-change as follows: when a ship bow travels over an abrupt, decreasing step in water depth, an upward facing velocity component is generated causing a positive wave. Oppositely, when the ship's bow travels over a water level increasing step, a downward-facing velocity component causes a depression wave.[31] When the ship stern passes the respective steps, the opposite sign waves are generated. An illustration of this generation mechanism is provided in Fig. 1(a). All the above-described, four wave components will travel as free waves with shallow water wave celerity. Grue, Pedersen, and Saetra[28] apply the same theoretical framework to a case of a thunderstorm propagating over the Norwegian trench. The close agreement of the derived analytical solution with the free surface elevation obtained from field data indicates a generation mechanism analogous to the ship wave generation at the Oslo fjord of these free waves when a barometric forcing travels over depth changes. These results hence document that depth-change induced waves of different origins (ships and barometric pressures) are the result of comparable generation mechanisms and exhibit resembling propagation characteristics.

So-called edge waves are generated when a disturbance travels parallel along an inclined coastline. Edge waves are a set of trailing waves following an initial disturbance as illustrated in Fig. 1(c). The characteristics of these trailing waves are dependent on the bathymetry slope, with forcing terms such as speed and diameter of the disturbing source, i.e., a weather system.[33] The longer the disturbance travels, the larger the area occupied by the edge waves. The phenomenon was mathematically derived by Greenspan[34] and is, therefore, called Greenspan resonance. Muscalus[23] compared field measurements from the Savannah River, US, with numerical simulations from a Boussinesq-type model and the analytical description of edge waves. The close agreement of the numerical results and the field data with the analytical description of edge waves indicate that large displacement ships can cause edge waves, a phenomenon until then described as a result of the displacement of barometric pressures. The results

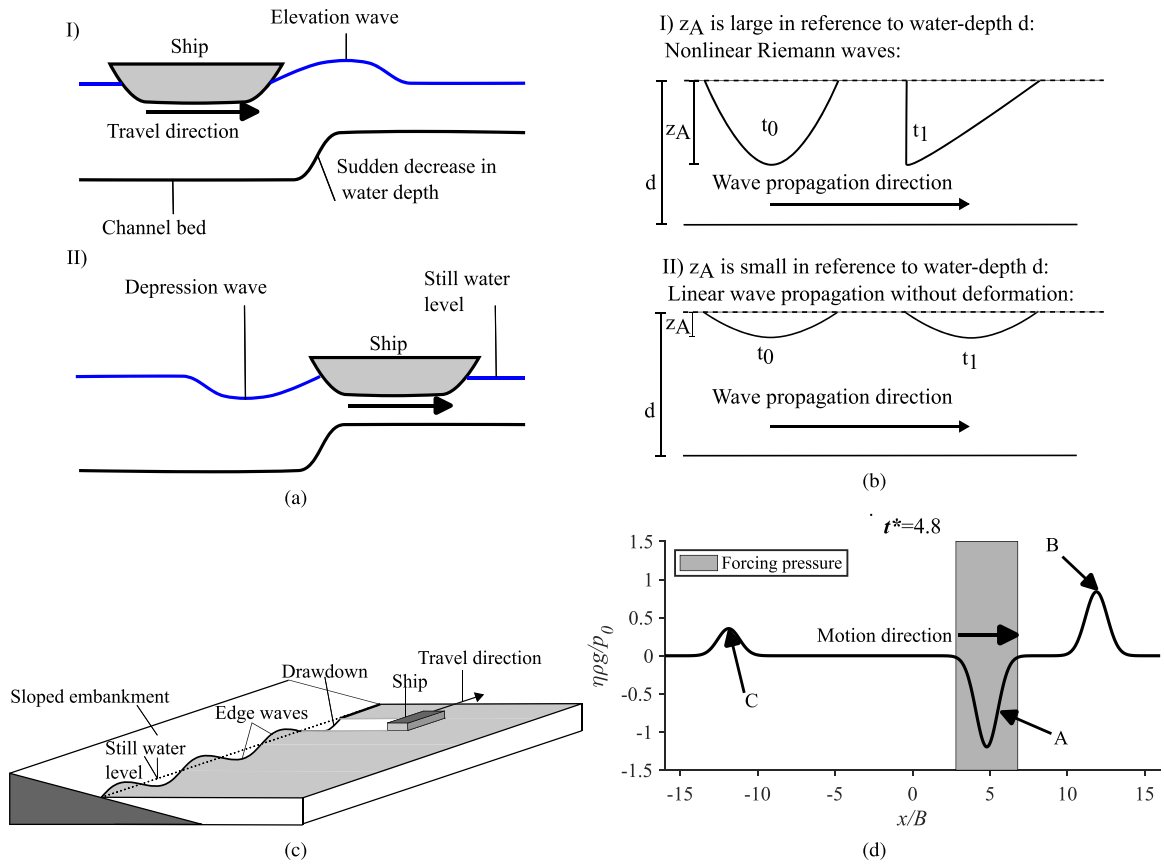

FIG. 1. Illustrations of the different shallow water effects governing the interaction of long-period bound waves considering different bathymetric attributes. (a) Free wave generation when a ship passes a sudden decrease in water depth. (a-I) The generation of an elevation wave when the bow passes the step and (a-II) indicates the depression wave when the stern passes the step. Redrawn after Ref. 28. (b) Wave deformation of progressing depression waves. (b-I) The nonlinear deformation following the theory of Riemann waves, causing asymmetric wave deformation leading to a steep rear slope. (b-II) The linear propagation absent of deformation in the case of small depression wave heights in relation to the water depth. Own illustration, following the work of Refs. 1, 3, 13, and 35. (c) Ship-induced edge waves when a vessel travels along a sloped embankment. Own illustration based on the work of Refs. 23 and 40. (d) Illustration of the different waves generated by an arbitrary moving pressure term in a one-dimensional system under sub-critical conditions at $F_d = 0.4$. The forced wave A, moving with the pressure term, the free wave B traveling in pressure term direction, and C the free wave traveling in opposing direction of the pressure term are clearly visible. In cases A and B travel with same speed ($F_d = 1$), their respective amplitudes increase (Proudman resonance).

hence further indicate that long-period ship waves and large scale waves from barometric origin are governed by analogous processes.

Wave deformation of ship-induced primary wave systems, in particular the drawdown, is well documented by Parnell *et al.*[1] and Rodin *et al.*[13] In cases where the amplitude of the drawdown is large in relation to the water depth, i.e., in cases of high non-linearity, the drawdown is found to deform during its propagation. While the drawdown is symmetric near the sailing line, the front slope gets increasingly milder in distance to its origin, while the rear slope steepens as depicted in Fig. 1(b). This observation is largely in agreement with the shallow water solution for highly nonlinear waves, so-called Riemann waves, known from analogous acoustic phenomena.[35]

Nonlinear waves are characterized by a dependence of the propagation speed on the wave height. In the case of depression waves, this means that the depression propagates slower than linear theory would suggest. The wave, hence, deforms over time and space, such that the front slopes get more gentle, while the rear slope steepens, due to the different celerity within the nonlinear wave. The steepening can eventually cause wave breaking and the formation of a bore, i.e., a step-like turbulent wave front, which is the result of a hydraulic jump in motion,[36,37] following the drawdown.[13] The deformation can further lead to shock-like waves at the rear slope, and its impact being relevant for design questions.[1]

In contrast to the previously introduced wave deformation following the theory of Riemann waves, the Proudman resonance essentially is a linear phenomenon.[32] As suggested by Williams *et al.*,[38] the idealized mathematical problem is referred to as strict Proudman resonance. In such a one-dimensional system, a forced wave—for example induced by a moving pressure term—causes three different waves: *A* a forced wave traveling with the forcing term's speed in its direction, *B* a free wave traveling with shallow water wave celerity in its direction, and *C* a free wave traveling in opposing direction to the forcing term;[38,39] the third wave is neglected in the present analysis. Fig. 1(d) illustrates these wave components, using the free surface elevation

normalized with the hydrostatic pressure head divided by a length scale normalized with the pressure term width B, for a sub-critically moving pressure term.

If the forced wave A travels at a slower speed than the free wave B, it is referred to as a sub-critical regime, while if the forced wave is faster than the free wave, it is referred to as supercritical regime. It is convenient to introduce a depth Froude number $F_d = \frac{v_p}{gd}$, where v_p denotes the forcing term speed, g is the gravitational acceleration, and d denotes the water depth. The sub-critical case is then described by $F_d < 1$ and the supercritical one by $F_d > 1$. In both cases, the forced and free waves travel at different speeds and separate from each other with progressing propagation distance. In a sub-critical case, a local increase in pressure causes a forced depression wave, while both free waves are positive.[39] In a supercritical regime, the forced waves are positive, while the forced wave is followed by a free depression wave.[39] In case the forced wave A travels with shallow water wave celerity, i.e., $F_d = 1$, the regime is referred to as critical. In this regime, the forced wave A and the free wave B travel at the same speed and cannot separate from each other, and the amplitude of both waves increases linearly with time.[41,42]

The linearity of this effect arises from the assumption that the free wave travels with shallow water wave celerity $c = \sqrt{gh}$. It is only valid when assuming that the wave height is relatively small compared to the water depth, i.e., $H \ll d$. Otherwise, wave deformation due to the different travel speeds of positive and depression wave would develop (amplitude dispersion).

So far, the Proudman resonance has only been documented to govern the wave amplitudes of meteotsunamis and landslide tsunamis.[41,43–45] Yet, given the analogies between long-period ship waves and barometrically forced waves (the previously outlined edge waves and wave generation at a step), it is hypothesized that an agreement of free and forced waves' speed (Proudman resonance) can also govern the propagation of long-period ship waves. Despite these specific assumptions underlying strict Proudman resonance, it could be shown by numerical simulations that the amplification in wave height is not limited to the exact agreement of free and forced wave speed. Even when relaxing the various assumptions underlying the mathematical derivation, an amplification of the wave height corresponding to Proudman's[32] theory is observed.[38] In particular, their results indicate that a range of critical Froude numbers exist, where a limited yet existent amplification is noted; its regime is thought to reside between $0.8 < Fh < 1.2$. Furthermore, their simulations indicate that the resonant amplification is not limited to one-dimensional cases but is also present in two-dimensions.[38] Yet, the underlying simulated cases show that the closer the simulated case is to a one-dimensional situation, i.e., the wider the forcing pressure term is, the larger the amplification effect gets.[38]

With the aim to study the wave making resistance of vessels moving in dredged channels, Beck, Newman, and Tuck[46] studied the added resistance due to shallow water regions using potential flow theory. The case examined consists of a vessel moving in a deep fairway while being symmetrically surrounded by shallow water regions with water depth d_{SW}. In between these regions, a step exists, causing an immediate change in water depth. Assuming that the ship travels in a sub-critical regime, while the shallow water regions correspond to supercritical conditions, the authors derived the velocity potential in the shallow water domains to be defined as

$$\Phi = \psi(x - \sqrt{F_{SW}^2 - 1} \cdot (y - y_c) \quad \text{for } y > y_c, \tag{1}$$

where the parameter Φ denotes the velocity potential, ψ denotes the stream function, x denotes the coordinate in ship motion direction, y denotes the coordinate normal to it, and y_c describes the distance in between the ship and the fairway boundary. The equation, hence, describes an upstream oriented wave, whose propagation direction is dependent on F_{SW}, the shallow water Froude number, setting the ship speed in relation to the water depth at the shallow outer area $F_{SW} = \frac{v}{\sqrt{gd_{SW}}}$.

C. Objectives

The aforementioned literature review indicates several knowledge gaps, as outlined in the following:

- In dredged channels surrounded by adjacent shallow water areas, a large propagation distance of ship-induced depression waves is reported.[1,2,7] The physical processes determining this unexpectedly high propagation distance are not yet understood.[3]
- The long-period ship wave system is found to travel in a different direction than the ship's sailing line.[2,7] To date, the parameters determining this primary wave propagation direction are not understood.[2,7]
- The amplitude of meteotsunamis and landslide tsunamis can be increased through resonant amplification, when the forcing term speed matches the shallow water wave celerity[41,43–45] (Proudman resonance[32]). Long-period ship waves exhibit analogies to these geophysical forced waves,[1,35] which covers other resonant phenomena as well (i.e., Greenspan resonance[23]). To date, it has not been examined if comparable resonant processes also affect the amplitude of long-period ship waves.

The objective of this article is to examine the far-field behavior of the primary wave system of ships moving near shallow water regions, as often present in the deepened waterways traveled by seagoing ships. Based on generic bathymetric configurations, potential reasons for the propagation of the ship-bound drawdown propagating in form of depression waves over large distances are examined by using numerical simulations based on nonlinear shallow water equations (NLSWE).

Specifically, the aforementioned outlined knowledge gaps are addressed by

- Analyzing the primary wave field in bathymetric configurations as outlined by Beck, Newman, and Tuck,[46] where the ship moves in a sub-critical regime, while its primary wave system moves in a supercritical regime.
- Examining the propagation direction of the primary wave system in shallow water areas.
- Investigating the influence of the water depth in shallow water on the propagation properties of ship-induced waves, to examine wave amplitudes in case of an agreement between free and forced wave celerities.

The remainder of the present article is organized as follows: In the following Sec. II, the numerical tool to simulate the propagation properties of the primary wave system is introduced and validated to ensure that the general resonant phenomenon is captured. A generic model setup to improve process understanding of ships moving near

shallow areas is introduced afterward. In Sec. III, numerical results obtained in the generic bathymetry are presented. A discussion then follows in Sec. IV, and before conclusions, and an outlook are presented in Sec. V.

II. MATERIAL AND METHODS

A. Research code REEF3D::SFLOW

To investigate long-period ship wave deformation in complex bathymetric environments, the shallow water-equation solver and module REEF3D::SFLOW are employed.[47,48] Recently, the free surface pressure term extension to approximate a ship hull's displacement in REEF3D::SFLOW has been intensively validated to accurately reproduce ship-induced wave generation.[26,49,50] Different shapes for the free surface pressure term can be used at the free surface to simulate ship wave generation, depending on the available data: a generic slender-body pressure term or a pressure field derived from real ship geometries.[50] Comparable models with a free surface pressure term extension are commonly found in studies of resonant phenomena during the propagation of meteotsunamis.[38,39,44] Similarly, models based on either NLSWE or the Boussinesq-equations using pressure term extensions are also used to study the generation and propagation of ship-induced waves.[12,25,51–53]

Depending on the focus of the examination, the modeling capacity for the simulation of frequency dispersion is of varying importance. In case short-period secondary ship waves need to be accounted for, models with an extended range of kh are preferred, including non-hydrostatic components such as multilayer SWE-models or Boussinesq models.[25,51–53] However, the primary wave system considered in this work is particularly long, such that frequency dispersion is of less concern as the ship length is large in relation to the water depth ($L_S \gg d$). At the same time, the stability when using a real ship hull is improved when using the numerically simpler NLSWE over non-hydrostatic SWE solvers or Boussinesq solvers.[50,54] In the present study, REEF3D::SFLOW is, therefore, employed in hydrostatic mode, as an extended range for kh up to π of the non-hydrostatic mode allowing the simulation of secondary waves[49] is not required. MacDonald[55] suggests a calculation of the deviation between the wave celerity in the numerical model c_{num} and the actual wave celerity c_{act} (and hence the importance of frequency dispersion effects) to be calculated as $\frac{c_{num}}{c_{act}} = \sqrt{1 + \frac{4\pi^2 d^2}{3L_S^2}}$. Applying this error metric to the given case suggests deviations between the REEF3D::SFLOW in hydrostatic mode and the actual wave celerities between 0.39% and 4.28%, which is considered satisfyingly accurate.

In the hydrostatic mode, the code's module REEF3D::SFLOW is based on depth-averaged versions of the continuity and momentum equations:[47,48]

$$\frac{\partial \eta}{\partial t} + \frac{\partial hu}{\partial x} + \frac{\partial hv}{\partial y} = 0, \tag{2}$$

$$\frac{\partial u}{\partial t} + u\frac{\partial u}{\partial x} + v\frac{\partial u}{\partial y} = -g\frac{\partial \eta}{\partial x}, \tag{3}$$

$$\frac{\partial v}{\partial t} + u\frac{\partial v}{\partial x} + v\frac{\partial v}{\partial y} = -g\frac{\partial \eta}{\partial y}. \tag{4}$$

In Eqs. (2)–(4), u and v are the depth-averaged velocities in the x and y directions, respectively. In the coordinate system, x and y denote the horizontal axes. The symbol t represents the time, d represents the still water depth, η is the free surface elevation, and $h = d + \eta$.

The governing equations are solved using high-order discretization approaches based on a finite differences method using a staggered and regular mesh. For the convective terms, a fifth order-accurate WENO scheme is employed, and the time-stepping algorithm is based on a third order-accurate TVD-Runge-Kutta explicit time-stepping approach. Numerical beaches can be considered by including relaxation zones to prevent reflection from the model boundaries.[47,56] Within the relaxation zones, the values for the surface elevations, velocities, and the pressure are smoothly decreased to zero at the outside of the domain following a relaxation function as suggested by Jacobsen, Fuhrman, and Fredsøe.[57] Wetting and drying is considered by setting the velocity in cells with a water level between a threshold corresponding to 0.001 m to zero.[47]

B. Validation study on Proudman resonance

To ensure that the numerical model REEF3D::SFLOW is capable of simulating resonant amplification, consistency with the literature is demonstrated by means of a simple one-dimensional test case. The waves generated by a moving pressure term are examined to allow a comparison between the analytical solution and numerical results obtained with the NLSWE solver. This one-dimensional validation test is chosen, as it is well established within the permanent literature. The pressure term speed corresponds with the shallow water wave celerity c, hence resonant amplification due to Proudman resonance can be expected.

In a one-dimensional domain of 20 000 m length with a depth of 10 m, a pressure function approximated as

$$f = \exp\left[-((x - v_p t)/B)^2\right] \tag{5}$$

is considered. Here, x denotes the spatial coordinate and B is the pressure term width set to $25d$. The pressure term is forced to move with a speed of $v_p = 9.9$ m/s, corresponding to $F_d = 1$. The parameters are chosen based on the ship dimensions studied in Sec. II C. The solution is compared to the linearized long-wave equation, given as[39,58]

$$\eta = \frac{dp_0}{2\rho c(c^2 - v_p^2)} \cdot \left[(c+v_p)f(x-ct) + (c-v_p)f(x+ct) - 2cf(x-v_p)\right], \tag{6}$$

where c denotes the shallow water wave celerity, p_0 denotes the initial pressure, and parameter ρ denotes the density. The free surface elevation η, normalized with the corresponding hydrostatic pressure head $p_0/\rho g$ over space, is examined at three time steps. The time steps are normalized with the pressure term width and speed, yielding the normalized time $t^* = t \cdot v/B$. The x axis denotes the normalized space, and the y axis denotes the normalized free surface elevation. Figure 2(a) shows the resulting normalized free surface elevation for a pressure $p_0/(\rho g d) = 0.001$, Fig. 2(b) shows a case with a pressure of $p_0/(\rho g d) = 0.05$. In the left column [Fig. 2(a)], excellent agreement between the numerical solution and the linearized analytical solution for the free surface elevation is obtained for all time steps. A significant increase in the wave amplitude can be observed as suggested by the theoretical framework,[32] indicating the accuracy of the numerical model to simulate resonant amplification. In the case underlying

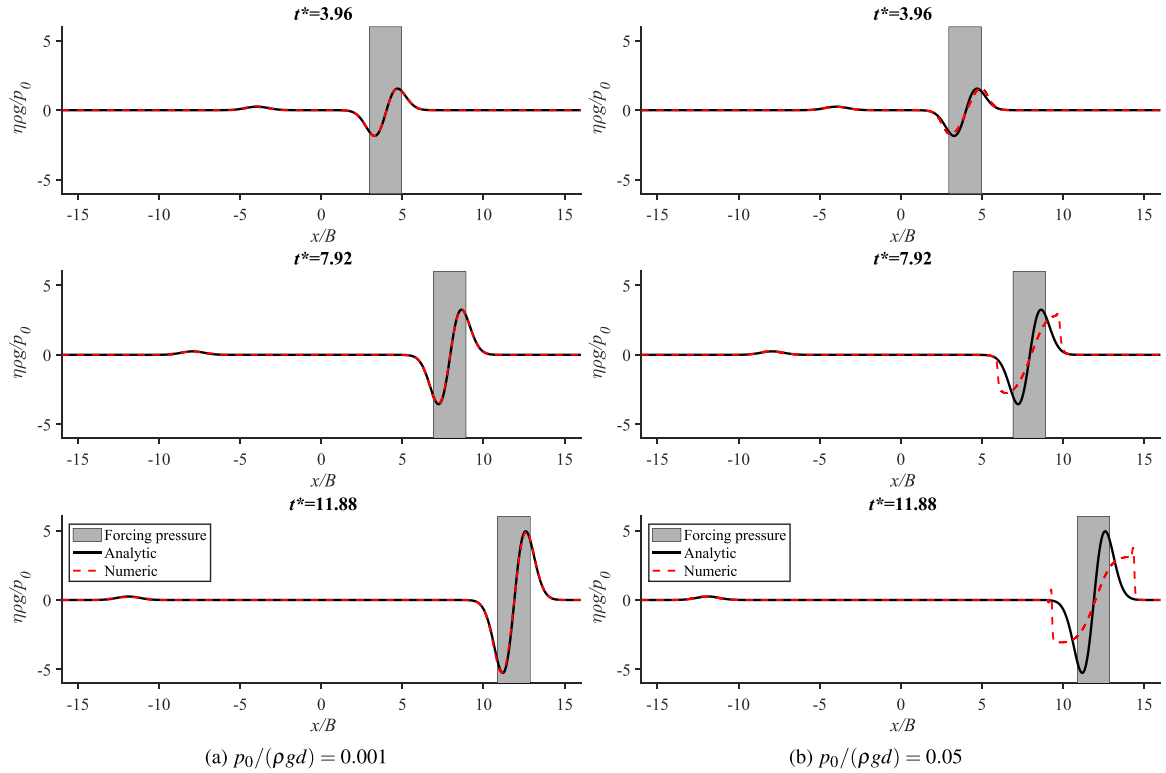

FIG. 2. The normalized free surface elevation over space at three distinct time steps t^* is shown. The normalized time step t^* is defined as $t^* = t \cdot v_p/B$ and, hence, describes the pressure term widths traveled at the respective time step. (a) A pressure of $p_0/(\rho g d) = 0.001$. (b) A pressure of $p_0/(\rho g d) = 0.05$. The free surface elevation resulting from a propagating pressure term obtained with the analytical solution of the linearized long-wave equation and by a numerical simulation with REEF3D::SFLOW are compared. The pressure term forcing speed corresponds to the shallow water wave celerity c; hence, an amplification of the wave amplitudes following Proudman resonance is expected and can be observed.

Fig. 2(b), the chosen initial pressure term is larger; hence, the wave amplitudes are increased. Correspondingly, this case is characterized by higher non-linearity, an effect that is expected to limit the resonant amplification and to result in nonlinear deformation of the individual wave components. Correspondingly, qualitative agreement between the analytical and numerical solution is only conserved for the first time step. At time steps 2 and 3, the wave amplitude continuously increases, resulting in increasing non-linearity and hence wave deformation. This deformation effectively limits the maximum wave heights, setting boundaries to the resonant amplification in cases of high non-linearity. The linear analytical equation does not account for such deformation, unlike the numerical model.

The nonlinear deformation present in this simple case underlying Fig. 2(b) corresponds to the wave deformation of nonlinear ship waves following the theory of Riemann waves.[1,13] When H/d becomes large, the wave height has an influence on the wave speed, causing a steepening of the front slope of positive waves and a steepening of the rear slope of negative waves. In contrast, the wave steepness is of less concern as the wavelength of ship-induced primary waves is particularly long.[6]

After establishing confidence in the numerical tool to simulate resonant effects, it is in a following step applied to a case of a ship propagating in a complex bathymetry.

C. Generic domain definition

To examine the far-field propagation properties of ship-induced primary waves, a conceptual case of a ship traveling along a shallow water (SW) area is examined. This bathymetric configuration even though highly simplified serves as a generic approximation of ships traveling through a deep fairway while being surrounded by a shallow water area. The setup is as general as possible to allow process understanding, rather than the representation of a specific waterway. In contrast, to the symmetric bathymetry suggested by Beck, Newman, and Tuck,[46] the shallow water area is only present at one side, to limit the impact of the SW-area on the channel cross section. Furthermore, in contrast to the analytical solution, symmetry is not required.

An illustration of the model case is presented in Fig. 3. An arbitrary ship is chosen, based on a physically plausible range of dimensions. The ship has a length L_S of 184.0 m, a beam B of 27.5 m, and a draft D of 5.0 m. It travels with a speed of $v = 9.9\,\mathrm{ms}^{-1}$. Due to the underlying specific dimensions of the vessel, normalized quantities tend to result in odd numbers.

The domain is split into two parts along a ship's sailing line. In the left part, cross section A is used, which means that the water depth is set to a uniform depth of $d = 4D$. After $54L_S$ waterway, cross section B is employed, which means that the water depth in a distance

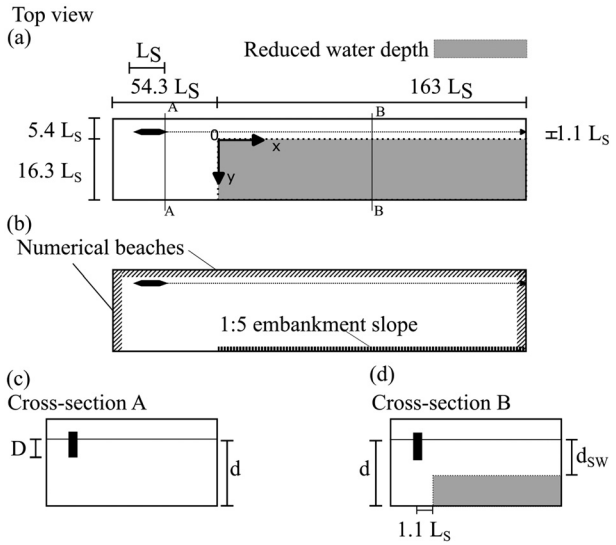

FIG. 3. Generic model setup for the numerical simulations used to understand ship wave deformation in shallow water areas adjacent to the fairway. In (a), the domain dimensions are shown in a top view, and the position of the shallow water area is indicated in gray color. In (b), the location of the numerical relaxation zones and the sloped embankment is shown in a top view. In (c), the cross section *A* is shown, and in (d), cross section *B* is depicted including the reduction of water depth. Not to scale.

$\Delta y = 1.1L_S$ to the ship sailing line is reduced to d_{SW}. In cross section *A*, the Froude number is maintained at a constant value of $F_{FW} = 0.7$. Different water depths are examined in the shallow water, corresponding to different target shallow water depth Froude numbers F_{SW}, while keeping the ship speed constant. The examined SW-Froude numbers fall within a range of 0.7–1.5. This implies that cases where the ship moves and the corresponding primary wave system moves in a sub-critical regime are examined as well as cases where the ship moves sub-critical, while the corresponding wave system moves supercritical. For the sake of brevity, the expression sub-critical and supercritical are used exclusively referring to the regime in the SW-zone. The depth within the shallow water zone is hence set to $d_{SW} = \frac{v^2}{F_{SW}^2 g}$. The free surface elevation is examined continuously at six transects parallel to the ship sailing line.

Numerical beach relaxation zones as introduced in Sec. II A are considered at three sides of the domain: the inlet, the outlet, and to the left of the ship. To the right of the ship, respectively, at the end of the shallow water zone, a sloped embankment with a gradient of 1 : 5 is considered. The grid size is set to 36 cells per wavelength ($dx = 5$ m) as determined by the convergence study given in Appendix, and the CFL number for the adaptive time-stepping is chosen as 0.3.

III. RESULTS

In this section, the results of the previously introduced generic model setup are examined focusing on the specific objectives outlined in Sec. I C, covering the propagation angles of ship-induced primary waves, the existence of resonant amplification, and the far-field propagation properties in distance to the ship.

A. Direction of the primary wave propagation

The primary wave system, as it evolves in space and time, is presented at first. Spatial distributions of the normalized free surface elevation from the simulation for five different SW-Froude numbers are depicted in Fig. 4. Qualitatively, different propagation properties can be seen for the sub-critical and the supercritical cases. In the sub-critical cases for $F_{SW} = 0.8$ and $F_{SW} = 0.95$, the primary wave system moves ship-bound and decays with distance to the ship, regardless of any influence of the shallow water area. In the supercritical cases, $F_{SW} = 1.05$ and $F_{SW} = 1.3$ and $F_{SW} = 1.5$, the water level does not reach the still water level, but a persistent primary wave system is visible over the entire SW-area. An exact quantification and subsequent discussion of this modified far-field wave system will be the focus of Secs. III B and IV. Furthermore, in the sub-critical regime, the primary wave system is symmetric to the centerline of the ship in the

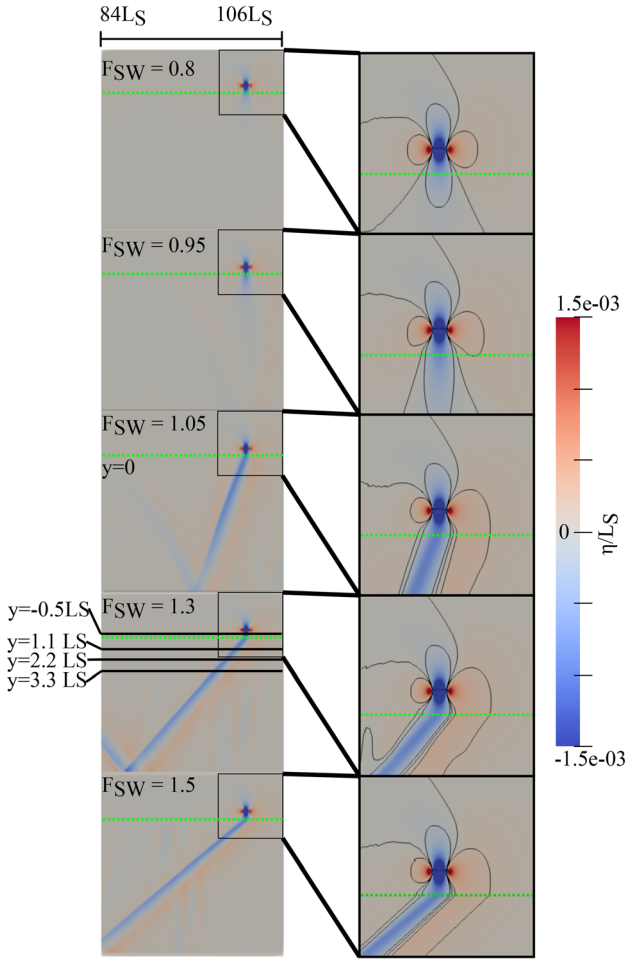

FIG. 4. Normalized free surface elevation η/L_S for different values of F_{SW}. The green line indicates the beginning of the SW area. The black lines for $F_{SW} = 1.3$ indicate the location of transects. The zoom boxes on the right side provide a detailed view on the deformation of the wave system at the beginning of the depth-transition and additionally show the contour lines corresponding to $\eta/L_S = -1.4 \times 10^{-4}$, 0 and 1.4×10^{-4}.

y-direction. This is no longer the case for the supercritical cases. Here, the directionality of the primary wave system changes at the SW-edge, such that the primary wave system lags behind the ship, causing a directional component of the primary wave system's propagation.

The observed directional component can be explained through a mismatch in the ship-velocity and the wave velocity. Under subcritical conditions, the primary wave system is moving ship-bound. However, in shallow water, the travel speed c of a wave is governed by the water depth. Assuming $h \ll d$, hence assuming that linear wave theories are valid, leads to the well-known expression $c = \sqrt{gh}$. If the wave celerity in the shallow areas is smaller than the ship speed, hence in supercritical cases, this leads to a discrepancy between the ship speed and the travel speed of its wave system. Therefore, the propagation direction of the primary wave system changes, such that the wave propagation normal to the crest matches the shallow water wave celerity. An illustration of these different directional components is given in Fig. 5. The angle of propagation between the primary wave and the ship sailing line is governed by the relation of the magnitude of the vectors c and v. A simple trigonometric consideration then yields

$$\Theta = \arcsin(c/v), \tag{7}$$

respectively

$$\Theta = \arcsin(1/F_{SW}). \tag{8}$$

Hence, at the location of the critical depth, the ship-bound drawdown generates free depression waves, propagating over the adjacent flats with a propagation direction deviating from the ship's sailing line. This directional description of the primary wave propagation under supercritical conditions agrees with the description of the generated free waves in the case of a supercritical "outer area" by Beck, Newman, and Tuck.[46] Furthermore, it should be noted that this propagation angle corresponds to the Havelock angle.[59]

Examining the propagation direction of the primary wave system for all supercritical cases studied in Fig. 6 confirms that the simulated propagation direction of the primary wave system corresponds to the analytically obtained ones by Eq. (8). This means that when the ship speed is supercritical in reference to the shallow water wave celerity,

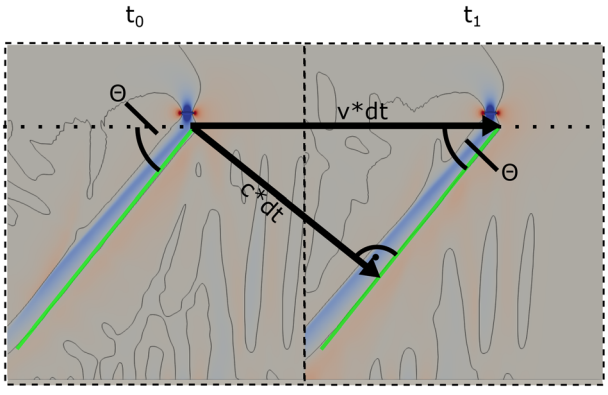

FIG. 5. Propagation direction of the supercritical primary wave system for $F_{SW} = 1.3$. The color code indicates the free surface elevation, and the contours indicate $\eta = 0$. The green line indicates the $\eta = 0$ between the bow wave and the drawdown.

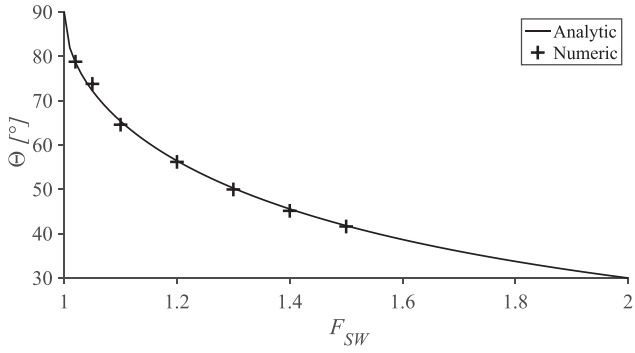

FIG. 6. Propagation direction of the supercritical primary wave system dependent on the shallow water depth Froude number.

the propagation speed of the primary wave system within the shallow water area always corresponds exactly to the shallow water wave celerity.

B. Amplitude of the primary waves

While the effect of the discrepancy on the qualitative wave field on the propagation direction in the supercritical area was examined in Sec. III A, the focus in this section is put on the quantification of the amplitude of the depression wave. To examine the effect of the SW-area on the simulated wave heights, the free surface elevation η is extracted at six transects parallel to the ship sailing line.

In Figs. 7(a)–7(c), the normalized free surface elevation η/L_S for $F_{SW} = 1.05$ over space is depicted at several discrete time steps. The time steps are chosen based on a normalization with the ship length and ship speed yielding $t^* = t \cdot v/L_S$ (see colorbar for coding). This implies that within each normalized time step, the ship travels one ship length. Each third normalized time step is shown within the figure. As indicated in Fig. 3, negative values for x/L_S imply that the ship travels in cross section A, before reaching the SW-area. The colorcode indicates the elapsed time, ranging from $t^* = -8$ when the ship travels in cross section A to $t^* = 61$. The black envelopes indicate the maximum drawdown that is reached at each specific point, during the simulation time. Figure 7(a) shows the normalized elevation at $y = -0.54L_S$, in the deep fairway before reaching the SW-area. It can be seen that the drawdown amplitude increases slightly. The increase can not be explained by shallow water effects but is probably a result of the modification of the channel's cross-sectional area and corresponding intensified confinement. At the edge of the shallow water area at $y = 0$ (location indicated as a green line in Fig. 4), depicted in Fig. 7(b), an increase in the drawdown amplitude sets in at $x/L_S = 0$. At $x/L_S = 8$, a constant amplitude is reached, which then remains constant. Figure 7(c) shows the spatial development of the primary wave system at a transect in $2.2L_S$-distance to the SW-Edge. The transect is chosen as a representation of the free surface development in the shallow water area. After an initial ramp-up distance lasting until $x/L_S = 28$, a depression wave amplitude corresponding to the one observed at the SW-edge is established.

Due to the small ship draft chosen, the nonlinear deformation of the wave shape is small, such that the shape of the wave signals at the different transects (a)–(c) agree qualitatively. Despite the chosen draft,

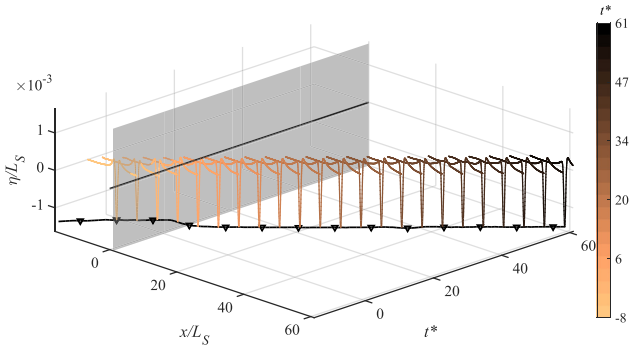

(a) Normalized free surface in the deep part between ship and edge ($y/L_S = -0.54$)

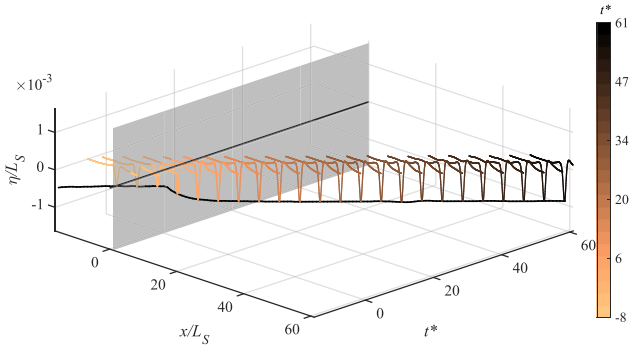

(b) Normalized free surface at $y/L_S = 0.0$, along the edge

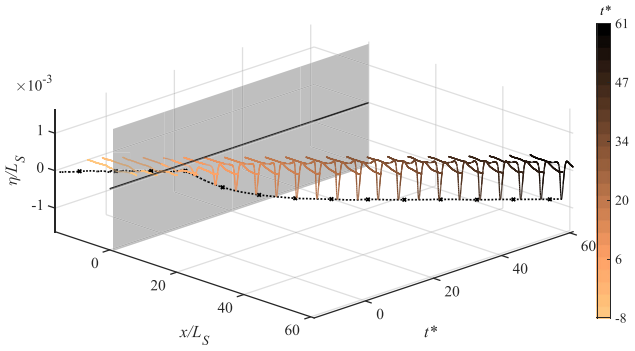

(c) Normalized free surface at $y/L_S = 2.2$

FIG. 7. Instantaneous free surface profiles for the ship-induced drawdown extracted at several discrete timesteps for $F_{SW} = 1.05$. The x axis denotes the normalized coordinate in the ship's motion direction, and the y axis denotes the normalized time step $t^* = t \cdot L_S/v$. Each third normalized time step is presented. The z axis denotes the non-dimensional free surface elevation. The gray area indicates the beginning of cross section *B*. The envelope curve describes the maximum drawdown amplitude over space. (a) The result at $y/L_S = -0.54$; (b) the result at the location $y/L_S = 0.0$; (c) the location $y/L_S = 2.2$.

some asymmetry of the depression wave can be observed at $y = 2.2L_S$, with a more gentle front slope and a steeper rear slope.

To allow the efficient examination of a larger set of simulation cases, the respective maximum normalized drawdown height z_A/L_S over space between $-15 < x/L_s < 61$ is examined in Figs. 8(a)–8(c). Due to the constant ship speed and the corresponding linear

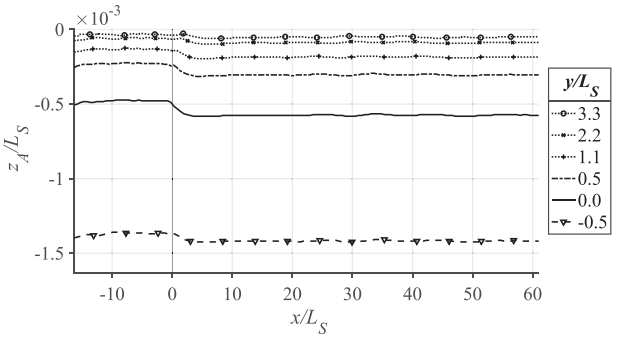

(a) $F_{SW} = 0.8$

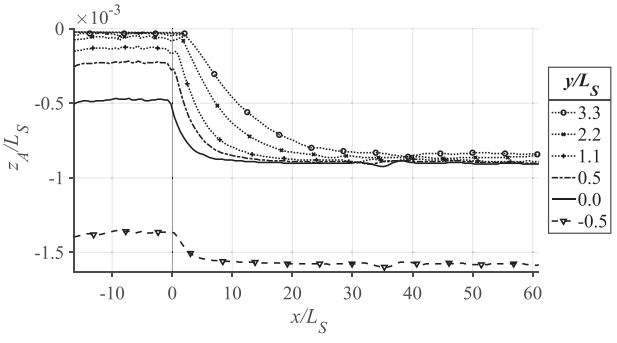

(b) $F_{SW} = 1.05$

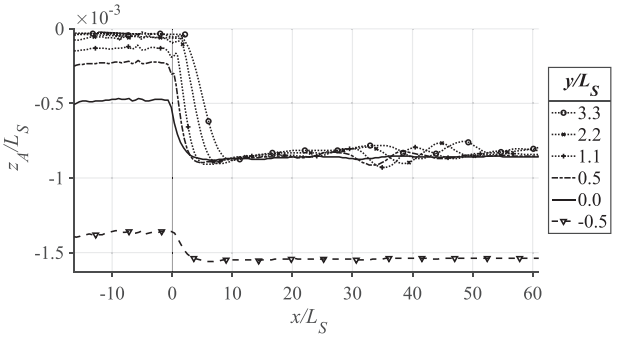

(c) $F_{SW} = 1.3$

FIG. 8. Spatial development of the normalized maximum drawdown amplitude z_A/L_S at different transects parallel to the sailing line. (a) The result for $F_{SW} = 0.8$; (b) the result for $F_{SW} = 1.05$; (c) the result for $F_{SW} = 1.3$. The individual curves for $y/L_S = -0.5, 0.0, 2.2$ in (b) correspond to the black envelopes included in Figs. 7(a)–7(c).

relationship between x and t^*, a two-dimensional presentation is chosen to allow a more detailed analysis of the drawdown height. Hence, z_A is defined as the deepest point of the drawdown to the still water level, which is reached within the simulated time and, hence, shows the development of the drawdown as the ship progresses in space and time. These correspond to the envelopes also included in Fig. 7, but additional transects at the distances $y/L_S = 0.5, 1.1, 3.3$ are also considered. Figure 8(a) shows the sub-critical case with a SW-Froude number of $F_h = 0.8$, Fig. 8(b) shows the supercritical case $F_h = 1.05$, and Fig. 8(c) shows the supercritical case $F_h = 1.3$.

For the sub-critical case $F_{SW} = 0.8$ shown in Fig. 8(a), the drawdown increases slightly at all transects once the ship enters cross section B, which can be explained through the higher channel blockage factor that comes with the reduced depth in the SW-zone. The development of the depression wave amplitude in the supercritical cases shown in Figs. 8(b) and 8(c) further supports the observations from Fig. 7. Once the ship enters cross section B, the drawdown amplitude increases until reaching a constant value. The maximum drawdown reached is mostly independent of the distance between the measurement location and SW-edge. The long-period oscillation between $30L_S$ and $50L_S$ is reflected wave components from the acceleration phase (precursor solitons[50]) as no beach was applied on the right side of the domain.

The point where the maximum depression height is reached depends on the SW-Froude number and the distance between the transect and the edge of the shallow water zone. The higher the SW-Froude number is, the sooner the maximum depression is reached. This in agreement with the different propagation angles. The larger the Froude number, the higher the difference in propagation direction of the ship and the induced depression waves, thus the larger the depression waves propagation component normal to the ship's sailing line.

The dependence of the drawdown on the SW-Froude number is shown in Fig. 9 for two different transects at $y = 0L_S$ and $y = 2.2L_S$.

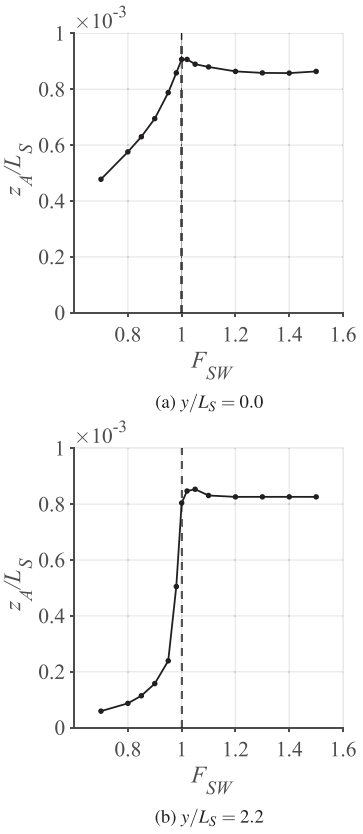

FIG. 9. Dependence of the quasi-stationary normalized drawdown amplitude reached within cross section B, on the SW-Froude number F_{SW}; dashed line indicates the limit of the critical regime. (a) The results at $y/L_S = 0.0$; (b) the results at $y/L_S = 2.2$.

In both subplots, the dependence is qualitatively similar: the drawdown increases with increasing SW-Froude number until reaching a plateau at Froude number of unity. This means at SW-Froude numbers higher than unity, the drawdown remains constant. This is in agreement with the directional velocities of the wave components. At supercritical conditions, the ship-velocity v deviates from the wave celerity c, such that the drawdown propagates as free depression wave with critical velocity c. At the location of the edge depicted in Fig. 9(a), a significant increase in the drawdown amplitudes in the near-critical regime can be observed. This is in agreement with the findings of Williams *et al.*,[38] indicating a range of Froude numbers, where free and forced waves travel at similar speeds. At the more distant location shown in Fig. 9(b) in contrast, a larger difference in the amplitudes between the sub- and supercritical regime can be observed. It is assumed that, in this sub-critical regime, close to the critical regime, an effect of the resonance on the wave amplitude takes place. Yet, no continuous free wave generation sets in, as the primary wave system still moves ship-bound, and no change in the motion direction of the wave system takes place (as can be seen in Fig. 4).

In order to study the propagation properties of ship-induced depression waves in more detail, the dependence of the wave height on the distance to the ship is analyzed in closer detail. In Fig. 10, the stationary drawdown height normalized with the drawdown height at $y = -0.5L_S$ is shown on the y axis, plotted against the normalized distance to the SW-edge y/L_S. Each line denotes a different simulation with a different SW-Froude number.

It can be seen that the wave dampening in supercritical and the sub-critical regime behaves qualitatively differently. In the sub-critical cases, the drawdown height decays quickly with distance to the ship. At $3.3L_S$-distance to the SW-edge, the drawdown is reduced below 10% of the initial drawdown height at $y = -0.5L$. In all supercritical cases, the depression magnitude is also reduced between $y = -0.5L$

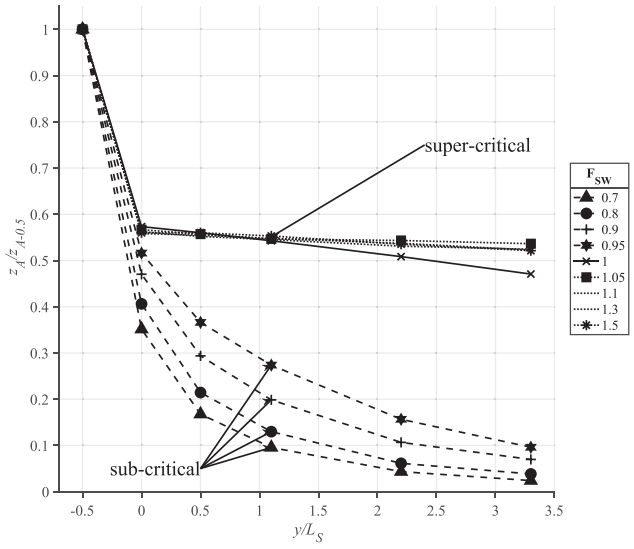

FIG. 10. Maximum drawdown amplitude dependent on the distance to the shallow water edge; the different regimes can be clearly differentiated: In the sub-critical regime, the drawdown quickly decays with distance to the edge; in the supercritical regime, the drawdown propagates with only minimal wave dampening.

and the edge at $y = 0$. However, in the entire shallow water zone, the reduction of wave height is only marginal, which implies that the depression magnitude at $y = 3.3L$, which is the most distant gauge analyzed, still corresponds to 90% of the one measured at $y = 0$.

IV. DISCUSSION

The far-field behavior of ship-induced depression waves, commonly generated by relatively large commercial vessels, has so far only partly been understood.[2,3,5] The above-presented evidence, originating from numerical simulations with a NLSWE-equation solver, suggests that even though these ships exclusively travel at sub-critical speeds in relation to the water depth at the fairway, their wave systems can travel at supercritical speeds as the water depth decreases near the embankments. In these situations, the ship-bound drawdown can travel as a depression wave over a much larger distance than previously assumed, as it propagates as a free wave in a direction that can deviate from the ship's motion trajectory. Despite the propagation of ship-induced depression wave being a multidimensional process, the propagation is essentially driven by an agreement of free and forced wave speeds, such that it can be described as a two-dimensional version of the Proudman resonance, which is in its strict formulation only applicable to one-dimensional cases. At the interface between sub and supercritical region (hence at the SW-edge at $y = 0$), the ship-bound drawdown and the free depression wave travel at the same speed in ship direction. A continuous energy transfer into the free wave, therefore, takes place, the surface disturbance is fed from the continuously provided energy offered from the ship's drive. However, as the free wave moves in a different direction than the ship, the free wave immediately loses contact to the forced wave's origin. In contrast, to the one-dimensional strict Proudman resonance, the supercritical depression wave propagation, therefore, does not lead to an intense amplification of the wave height, but rather to an increased propagation distance of the depression wave. Essentially, the depression wave travels as a one-dimensional wave normal to its wave crest, such that no lateral decay takes place. Yet, as this propagation direction deviates from the sailing line, a two dimensional approach is necessary for their simulation; unlike the strict one-dimensional Proudman resonance, a numerical model instead of sets of equations is required to govern the wave propagation.

During generation and propagation of ship-induced depression waves, this work gives evidence that several phenomena interact. The waves' generation itself is driven by Bernoulli's conservation law, and the shape during their propagation is further driven by nonlinear effects.[1,13] As a consequence, it is difficult to isolate the underlying processes in field measurements alone due to complex bathymetric features overriding the strict physics, while experimental methods often lack the required space to reproduce the deformation as studied within the given article. In the numerical simulations presented herein, the far-field propagation of ship-induced wave heights due to the sub/supercritical mismatch of propagation speed is isolated from these other effects, as much as possible. In turn, this includes assumptions that differentiate the generic test case from conditions in real waterways, as discussed in the following.

A navigation situation where a deep channel is surrounded by shallow water areas is relatively common (e.g., Refs. 1, 2, 12, and 22). However, none of these cases considers a vertical step, between the fairway and the SW-area. This step potentially conflicts with shallow water approximations, as vertical velocity accelerations can reach an order of magnitude as the horizontal ones. Yet, as discussed by Beck *et al.*[46] based on the work of Lamb[60] and Bartholomeusz,[61] due to the long wavelength of the governing wave system, the assumptions of shallow water theory can still be considered valid. The step is, therefore, chosen, as it provides sharp differentiation between the sub and supercritical areas. Furthermore, a completely flat SW-area is a special case that is only characteristic for certain waterways (e.g., the Venice Lagoon) at other waterways a shallow slope would typically be present (e.g., the Elbe estuary).[14] However, considering such a slope in the numerical simulations (not shown here) did not show a significant impact on the SW-area. On an inclined slope, the wave crests do not develop in a straight line, but they take a curved shape as the wave speed, and therefore, propagation direction changes with decreasing water depth. At the same time, a decreasing water depth would inevitably increase the non-linearity, leading to wave deformation or even breaking, an effect not wanted as it is the goal of the conceptual setup to isolate the critical far-field wave propagation from other effects as much as possible. It is further noted that considering different roughness parameters did not show to have any notable impact on the measured wave heights (not shown here).

A further assumption is that the bathymetry in cross section B is constant and not changing in the ship's motion direction. As discussed in Sec. III A, the location where a stationary depression is reached depends on the SW-Froude number and the distance to the SW-edge. The distance between the beginning of the cross section B and the stationary depression can be significant. This means that situations where the bathymetry changes negligibly in motion direction are more prone to far-field depression wave propagation. Yet, it is not necessarily required that a quasi-stationary situation is reached in order for the depression waves to exhibit their damage potential.

Despite these above-mentioned limitations, it seems very likely that the far-field wave propagation is to a large extent governed by the critical far-field wave propagation in many application cases. As the phenomenon is not limited to the critical SW-Froude number but occurs as soon as the primary wave system enters supercritical areas, corresponding navigation conditions are likely to occur frequently. An example case is provided in the following, to illustrate how the sub-supercritical mismatch can, indeed, contribute to fairly different wave loads even without the assumptions of the generic study but under realistic complex navigation conditions. A real bathymetry is extracted from the outer Weser estuary, a waterway traveled by container ships to reach the port of Bremerhaven, Germany.[62] The considered case is based on a *PPM40* vessel with a beam of 40 m, a length of 277 m, and a draft of 11 m, sailing with 7 m/s. In the examined stretch of the waterway whose geo-reference is provided in Fig. 11, the bathymetry is complex, including groins, a training dam, and underwater ripples, varying fairway widths and depths, varying distances to the depth isoline where $F_{SW} = 1$, and varying embankment slopes. Hence, all the previously discussed simplifications that are underlying the generic case are now replaced by realistic, yet complex estuarine conditions. There is no artificial step within the bathymetry, the SW-area is not completely flat, the slopes of the fairway have a varying inclination, and the bathymetry changes along the ship's motion direction. As the waterway is affected from tidal water level fluctuations, two cases with two different water levels are examined. One is assumed to be at −1.41 m below mean sea level, and the second one has a waterlevel of 2.59 m above mean sea level. The specific water levels are chosen for illustration purposes, such that for the lower water level, the

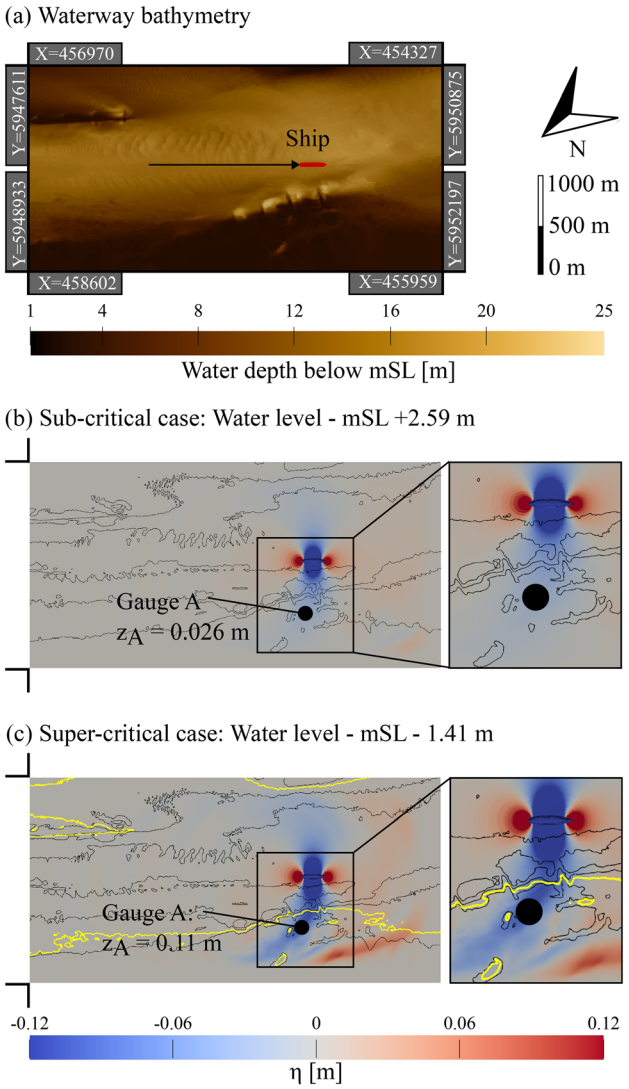

FIG. 11. Case study of a PPM 40 ship traveling through a complex bathymetry of the outer Weser estuary as shown in subfigure (a). The free surface elevation η from the simulation with a high tidal water level leading to a sub-critical navigation condition (b) is compared against a simulation of the same ship with the same speed, where a low tidal water level causes a supercritical outer area (c). The black contour lines indicate water depths of 13.59, 8.59, and 2.59 m below mean sea level, and the yellow contour line indicates the water depth where $F_{SW} = 1$. The coordinates in (a) are provided as UTM-coordinates for UTM zone 32U.

SW-region is characterized by a supercritical regime (the case is, therefore, referred to as supercritical case in the following), while in the case of the high water level, the entire domain is in a sub-critical regime (therefore referred to as sub-critical case). Numerical beaches are considered on all four sides of the domain, and the grid size is kept at a constant value of $dx = 5$ m.

Figure 11 illustrates the simulation results for the above-mentioned two cases. The color code represents the free surface elevation η. The black contour lines indicate water depths of 13.59, 8.59 and 2.59 m below the mean sea level. The yellow contour line represents the water depth contour where $F_{SW} = 1$ in the supercritical case. As expected, qualitatively different wave fields can be observed in the two cases examined. While the surface elevation in vicinity of the ship hull and to the left of the vessel (with reference to the heading) is largely unaffected by the change in water level, the drawdown to the right of the ship is much more pronounced in the case of the supercritical case compared to the sub-critical case. When the drawdown passes the yellow contour line, it lags the ship and remains at a relatively constant wave height in the supercritical case, agreeing with the expectation of its propagation speed and height. In contrast to the generic case, the outer boundaries of the drawdown do not form a straight line but rather take a spatially varying curved shape due to varying bed slopes and varying distances between the ship and the contour line. At the location of gauge A, in $2L_S$ distance to the ship sailing line and $0.6L_S$ distance to the location where $F_{SW} = 1$, the drawdown of the supercritical case (a) is four times higher than in the sub-critical case. While the exact analysis of the wave field would require a much more thorough analysis, this example shows that even when relaxing the idealized assumptions underlying the generic model setup of Sec. II C, a relevant effect from the sub-supercritical mismatch on the expected drawdown height, hence loads, can be expected in application cases.

Semi-empirical approaches assumed the FW-Froude number, the ship dimensions, the blockage factor, and the distance between the ship and the gauge location to be the most determining parameters for the long-period ship-induced loads (e.g., Refs. 8 and 63). The findings on the supercritical far-field propagation partially conflicts with considering the distance between the sailing line and the gauge as a determining parameter for predicting the long-period ship-induced loads. In this light, the primary wave generation as a result of the ship's displacement and accordingly the FW-Froude number and the channel blockage factor still seem plausible predictors for the primary wave height in the sub-critical parts of the fairway. In areas characterized by supercritical propagation, these parameters still play a decisive role, as the supercritical propagation describes a reduced decay of wave heights along supercritical areas rather than an increase in amplitude. The distance between the ship sailing line and the gauge, however, needs to be viewed critically, as the propagation properties are dependent on the location where the shift from the sub-critical to the supercritical regime takes place.

In addition, the far-field propagation is also governed by nonlinear deformation, eventually leading to wave breaking. In the present analysis, the effect of nonlinear deformation is purposefully excluded from the analysis to look at the supercritical far-field propagation specifically. However, for practical questions, the most critical wave loads are typically the highest, hence most nonlinear wave components. At the same time, wave breaking is described as a function of wave height to water depth,[13] which implies that the largest drawdown heights near the ship or at the location $F_{SW} = 1$ do not necessarily lead to the largest loads in distance to the ship, as wave breaking effectively limits the depression wave height. This implies that in the far-field, the depression wave height is less sensitive to ship parameters, since waves of smaller amplitude travel with less dampening, and larger waves are prone to a height reduction due to nonlinear deformation and breaking. This assumption is in agreement with the findings of Scarpa *et al.*,[2] whose measurements in the Venice Lagoon indicate that in 800 m distance to the ship, the depression wave height is in the same range for all ships traveling the waterway.

Finally, as highlighted by previous authors,[1,27] long-period ship-induced waves exhibit several analogies to waves arising from natural hazards. In contrast to these events, ship passages are frequent and can be planned, such that their wave system can comparably easily be measured. Improving the process understanding of the ship wave system can, therefore, be used to obtain field data that contribute to the process understanding of the more harmful threats due to landslide tsunamis and meteotsunamis.

V. CONCLUSIONS AND OUTLOOK

Based on the numerical results presented here, the following conclusions can be drawn:

- The far-field propagation properties of the ship-induced primary wave system in fairways surrounded by shallow areas can be governed by a mismatch between the sub-critical ship speed and the critical primary wave propagation speed.
- In case of a mismatch between the ship speed and the shallow water wave celerity, the ship-induced drawdown propagates as a free wave and its propagation direction dependent on the local depth Froude number in shallow water.
- In the absence of nonlinear effects, these drawdown-induced depression waves can travel over large distances, with only minimal height decay, leading to large depression wave heights several ship-lengths away from the sailing line.
- For the analysis of critical wave loads, further processes such as nonlinear deformation and wave breaking also need to be considered in the analysis.

Based on the presented work, process understanding of far-field propagation properties of long-period ship waves is improved. To derive conclusions for practical design questions, several future steps are required. So far, the mismatch between semi-empirical approaches and measurement is often relatively large for long-period ship waves when these travel in complex bathymetries.[8] Based on the improved process understanding, new parameters such as the distance between the ship sailing line and the critical SW-Froude number can be considered in novel semi-empirical approaches to predict the ship-induced loads. This also includes further research on the nonlinear deformation of depression waves. To date, no precise threshold is defined at which a forced depression wave can be considered linear or nonlinear.

The propagation direction of the depression wave deviating from the ship's motion direction indicates that reflections occur near the waterways embankments. They were outside the scope of the present analysis; however, a superficial analysis of the propagation direction indicated that the relation is relatively simple: the angle of the inbound wave corresponds to the angle of the reflected waves. However, the existence of wave reflections indicates that exactly at the banks, the superposition of incoming and reflective wave components is taking place, potentially increasing the damage potential of long-period ship wave on the embankments or structures near the embankments.[14,18] Therefore, further research on these reflections would be relevant for design purposes.

ACKNOWLEDGMENTS

This study is part of the research project NumSilaSu conducted in cooperation with the German Federal Waterways Engineering and Research Institute (BAW).

AUTHOR DECLARATIONS

Conflict of Interest

The authors have no conflicts to disclose.

Author Contributions

León-Carlos Dempwolff: Conceptualization (lead); Data curation (lead); Formal analysis (equal); Investigation (lead); Methodology (lead); Validation (lead); Visualization (lead); Writing – original draft (lead). **Christian Windt:** Conceptualization (equal); Data curation (equal); Formal analysis (equal); Investigation (equal); Writing – review & editing (equal). **Gregor Melling:** Conceptualization (equal); Data curation (equal); Formal analysis (equal); Investigation (equal); Writing – review & editing (equal). **Ingrid Holzwarth:** Conceptualization (equal); Funding acquisition (equal); Project administration (equal); Writing – review & editing (equal). **Hans Bihs:** Methodology (equal); Software (lead); Writing – review & editing (equal). **Nils Goseberg:** Conceptualization (equal); Funding acquisition (equal); Project administration (equal); Resources (equal); Supervision (equal); Writing – review & editing (equal).

DATA AVAILABILITY

The data that support the findings of this study are available from the corresponding author upon reasonable request.

APPENDIX: CONVERGENCE STUDY

The appropriate computational mesh is chosen based on a convergence study running simulations with four different mesh sizes corresponding to 18, 24, 36, and 48 cells per wavelength. The convergence study uses the case with a Froude number of $F_{SW} = 1.1$. The analyzed quantity is the drawdown at the edge ($Z_{A,0}$) after it reaches a quasi-stationary height in cross section B. The results are analyzed using an approach by Viola *et al.*,[64] which was

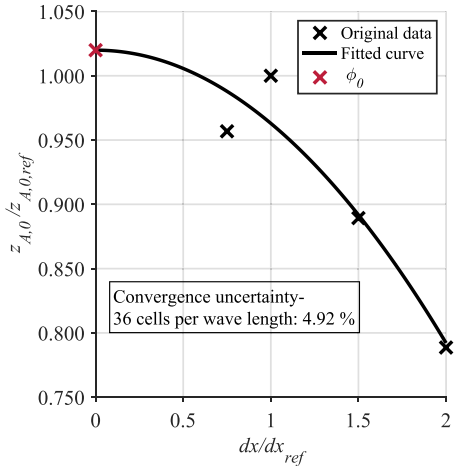

FIG. 12. Convergence study for the computational mesh following an extrapolation approach suggested by Viola *et al.*[64] ϕ_0 denotes the extrapolated normalized value for $z_{A,0}$ at infinitesimally small grid size.

also previously used within the validation of REEF3D::SFLOW.[50] The underlying idea of the approach is to extrapolate the results for the four computational meshes to obtain the value for an infinitesimal small grid (ϕ_0), using a quadratic fit. The grid uncertainty for the chosen grid is then estimated by forming the sum of the deviation between the value for $Z_{A,0}$ at the chosen grid and the extrapolated value ϕ_0, considering a safety factor of 1.25 and the standard deviation σ of the fit through all underlying data-points. The discretization uncertainty is hence provided as $err_{dx} = 1.25\Delta\phi + \sigma$.

In Fig. 12, the resulting data are given for the four examined meshes. The x axis shows the cell size normalized with the cell size of the chosen mesh. The y axis shows the respective value for the drawdown $z_{A,0}$, again normalized with the value for $z_{A,0,ref}$ at the chosen grid size. The chosen grid corresponds to 36 cells per wavelength, which is considered a good balance between the discretization uncertainty of 4.9% and the computational simulation time of 34 h on 20 AMD EPYC cores with 2.80 GHz.

REFERENCES

[1]K. E. Parnell, T. Soomere, L. Zaggia, A. Rodin, G. Lorenzetti, J. Rapaglia, and G. M. Scarpa, "Ship-induced solitary Riemann waves of depression in Venice Lagoon," Phys. Lett. A **379**, 555–559 (2015).

[2]G. M. Scarpa, L. Zaggia, G. Manfè, G. Lorenzetti, K. Parnell, T. Soomere, J. Rapaglia, and E. Molinaroli, "The effects of ship wakes in the Venice Lagoon and implications for the sustainability of shipping in coastal waters," Sci. Rep. **9**, 19014 (2019).

[3]K. E. Parnell, L. Zaggia, T. Soomere, G. Lorenzetti, and G. M. Scarpa, "Depression waves generated by large ships in the Venice lagoon," J. Coastal Res. **75**, 907–911 (2016).

[4]T. Soomere, "Nonlinear components of ship wake waves," Appl. Mech. Rev. **60**, 120–138 (2007).

[5]L.-C. Dempwolff, G. Melling, C. Windt, O. Lojek, T. Martin, I. Holzwarth, H. Bihs, and N. Goseberg, "Loads and effects of ship-generated, drawdown waves in confined waterways - A review of current knowledge and methods," J. Coastal Hydraul. Struct. **2**, 46 (2022).

[6]V. Bertram, *Practical Ship Hydrodynamics* (Elsevier, 2012).

[7]J. Rapaglia, L. Zaggia, K. Ricklefs, M. Gelinas, and H. Bokuniewicz, "Characteristics of ships' depression waves and associated sediment resuspension in Venice Lagoon, Italy," J. Mar. Syst. **85**, 45–56 (2011).

[8]B. Almström and M. Larson, "Measurements and analysis of primary ship waves in the Stockholm archipelago, Sweden," J. Mar. Sci. Eng. **8**, 743 (2020).

[9]C. L. Everett, O. Williams, E. Ruggiero, M. Larner, R. Schaefer, M. Malej, F. Shi, J. Bruck, and J. A. Puleo, "Ship wake forcing and performance of a living shoreline segment on an estuarine shoreline," Front. Built Environ. **8**, 917945 (2022).

[10]S. Gharbi, G. Valkov, S. Hamdi, and I. Nistor, "Numerical and field study of ship-induced waves along the St. Lawrence Waterway, Canada," Nat. Hazards **54**, 605–621 (2010).

[11]D. H. Schoellhamer, "Anthropogenic sediment resuspension mechanisms in a shallow microtidal estuary," Estuarine, Coastal Shelf Sci. **43**, 533–548 (1996).

[12]C. E. Bluteau, A. Van Rooijen, P. Matte, and D. Dumont, "Impacts of ship-induced waves along shorelines during flooding events," J. Waterw., Port, Coastal, Ocean Eng. **149**, 04023015 (2023).

[13]A. Rodin, T. Soomere, K. E. Parnell, and L. Zaggia, "Numerical simulation of the propagation of ship-induced Riemann waves of depression into the Venice Lagoon," Proc. Est. Acad. Sci. **64**, 22 (2015).

[14]G. Melling, H. Jansch, B. Kondziella, K. Uliczka, and B. Gaetje, "Damage to rock groynes from long-period ship waves: Towards a probabilistic design method," in Proceedings of the Coastal Structures Conference, Hannover, Germany (2019).

[15]G. Melling, H. Jansch, B. Kondziella, K. Uliczka, and B. Gaetje, "Evaluation of optimised groyne designs in response to long-period ship wave loads at Juelssand in the Lower Elbe Estuary," Die Kueste **89**, 28 (2020).

[16]D. Taylor, K. Hall, and N. MacDonald, "Investigations into ship induced hydrodynamics and scour in confined shipping channels," J. Coastal Res. **50**, 491–496 (2007).

[17]A. Seemann, G. Melling, H. Jansch, and B. Kondziella, "A design method for rock groynes exposed to overtopping from long-period ship wave loads," J. Coastal Hydraul. Struct. **3**, 1 (2023).

[18]L.-C. Dempwolff, C. Windt, G. Melling, H. Bihs, I. Holzwarth, and N. Goseberg, "Ship wave–induced hydraulic loading on estuarine groins: A conceptual numerical study," J. Waterw., Port, Coastal, Ocean Eng. **149**, 04023002 (2023).

[19]A. Silinski, M. Heuner, J. Schoelynck, S. Puijalon, U. Schröder, E. Fuchs, P. Troch, T. J. Bouma, P. Meire, and S. Temmerman, "Effects of wind waves versus ship waves on tidal marsh plants: a flume study on different life stages of *Scirpus maritimus*," PLoS One **10**, e0118687 (2015).

[20]B. Almström, P. Danielsson, G. Göransson, C. Hallin, and M. Larson, "Experiences of nature-based solutions for mitigating ship-induced erosion in confined coastal waters," Ecol. Eng. **180**, 106662 (2022).

[21]C. Houser, "Relative importance of vessel-generated and wind waves to salt marsh erosion in a restricted fetch environment," J. Coastal Res. **262**, 230–240 (2010).

[22]L. Zaggia, G. Lorenzetti, G. Manfé, G. M. Scarpa, E. Molinaroli, K. E. Parnell, J. P. Rapaglia, M. Gionta, and T. Soomere, "Fast shoreline erosion induced by ship wakes in a coastal lagoon: Field evidence and remote sensing analysis," PLoS One **12**, e0187210 (2017).

[23]A. C. Muscalus, "Characterization of low-frequency ship wake along the margins of confined channels and connected waterways," Ph.D. dissertation (Georgia Institute of Technology, 2022).

[24]D. Jong, D. Roelvink, S. Reijmerink, and C. Breederveld, "Numerical modelling of passing-ship effects in complex geometries and on shallow water," in Smart Rivers Conference, Liege, Belgium, Maastricht, Netherlands, 2013.

[25]B. Almström, D. Roelvink, and M. Larson, "Predicting ship waves in sheltered waterways – An application of XBeach to the Stockholm Archipelago, Sweden," Coastal Eng. **170**, 104026 (2021).

[26]L.-C. Dempwolff, C. Windt, H. Bihs, G. Melling, I. Holzwarth, and N. Goseberg, "Hydrodynamic coupling of multi-fidelity solvers in REEF3D with application to ship-induced wave modelling," Coastal Eng. **188**, 104452 (2024).

[27]I. Didenkulova, E. Pelinovsky, and T. Soomere, "Can the waves generated by fast ferries be a physical model of tsunami?" Pure Appl. Geophys. **168**, 2071–2082 (2011).

[28]J. Grue, G. K. Pedersen, and O. Saetra, "Free Wave Effects in Meteotsunamis," JGR Oceans **127**, e2021JC017669 (2022).

[29]A. C. Muscalus and K. A. Haas, "Vessel wake contributions to erosion at exposed and sheltered shorelines near a tidal shipping channel," Coastal Eng. **178**, 104220 (2022).

[30]J. Grue, "Ship generated mini-tsunamis," J. Fluid Mech. **816**, 142–166 (2017).

[31]J. Grue, "Mini-tsunami made by ship moving across a depth change," J. Waterw., Port, Coastal, Ocean Eng. **146**, 04020023 (2020).

[32]J. Proudman, "The effects on the sea of changes in atmospheric pressure," Geophys. J. Int. **2**, 197–209 (1929).

[33]C. An, P. L.-F. Liu, and S. N. Seo, "Large-scale edge waves generated by a moving atmospheric pressure," Theor. Appl. Mech. Lett. **2**, 042001 (2012).

[34]H. P. Greenspan, "The generation of edge waves by moving pressure distributions," J. Fluid Mech. **1**, 574 (1956).

[35]I. Didenkulova, E. Pelinovsky, and A. Rodin, "Nonlinear interaction of large-amplitude unidirectional waves in shallow water," Est. J. Eng. **17**, 289 (2011).

[36]H. Chanson, "Current knowledge in hydraulic jumps and related phenomena. A survey of experimental results," Eur. J. Mech. B **28**, 191–210 (2009).

[37]H. Von Häfen, C. Krautwald, H. Bihs, and N. Goseberg, "Dam-break waves' hydrodynamics on composite bathymetry," Front. Built Environ. **8**, 877378 (2022).

[38]D. A. Williams, K. J. Horsburgh, D. M. Schultz, and C. W. Hughes, "Proudman resonance with tides, bathymetry and variable atmospheric forcings," Nat. Hazards **106**, 1169–1194 (2021).

[39]G. G. Dogan, E. Pelinovsky, A. Zaytsev, A. D. Metin, G. Ozyurt Tarakcioglu, A. C. Yalciner, B. Yalciner, and I. Didenkulova, "Long wave generation and coastal amplification due to propagating atmospheric pressure disturbances," Nat. Hazards **106**, 1195–1221 (2021).

[40]X. Niu, "Conditions for the occurrence of notable edge waves due to atmospheric disturbances," Appl. Ocean Res. **101**, 102255 (2020).
[41]S. Tinti, E. Bortolucci, and C. Chiavettieri, "Tsunami excitation by submarine slides in shallow-water approximation," Pure Appl. Geophys. **158**, 759–797 (2001).
[42]I. Didenkulova and E. Pelinovsky, "Analytical solutions for Tsunami waves generated by submarine landslides in narrow bays and channels," Pure Appl. Geophys. **170**, 1661–1671 (2013).
[43]S. Monserrat, I. Vilibić, and A. B. Rabinovich, "Meteotsunamis: Atmospherically induced destructive ocean waves in the tsunami frequency band," Nat. Hazards Earth Syst. Sci. **6**, 1035–1051 (2006).
[44]I. Vilibic, "Numerical simulations of the Proudman resonance," Cont. Shelf Res. **28**, 574–581 (2008).
[45]I. I. Didenkulova, I. F. Nikolkina, and E. N. Pelinovsky, "Resonant amplification of tsunami waves generated by an underwater landslide," Dokl. Earth Sci. **436**, 66–69 (2011).
[46]R. F. Beck, J. N. Newman, and E. O. Tuck, "Hydrodynamic forces on ships in dredged channels," J. Ship Res. **19**, 166–171 (1975).
[47]W. Wang, T. Martin, A. Kamath, and H. Bihs, "An improved depth–averaged nonhydrostatic shallow water model with quadratic pressure approximation," Numer. Methods Fluids **92**, 803–824 (2020).
[48]W. Wang, A. Kamath, T. Martin, C. Pákozdi, and H. Bihs, "A comparison of different wave modelling techniques in an open-source hydrodynamic framework," J. Mar. Sci. Eng. **8**, 526 (2020).
[49]L.-C. Dempwolff, C. Windt, N. Goseberg, T. Martin, H. Bihs, and G. Melling, "Verification of a free-surface pressure term extension to represent ships in a non-hydrostatic shallow-water-equations solver," J. Offshore Mech. Arct. Eng. **145**, 021202 (2023).
[50]L.-C. Dempwolff, C. Windt, G. Melling, T. Martin, H. Bihs, I. Holzwarth, and N. Goseberg, "The influence of the hull representation for modelling of primary ship waves with a shallow-water equation solver," Ocean Eng. **266**, 113163 (2022).
[51]C. G. David, V. Roeber, N. Goseberg, and T. Schlurmann, "Generation and propagation of ship-borne waves - Solutions from a Boussinesq-type model," Coastal Eng. **127**, 170–187 (2017).
[52]C. Forlini, R. Qayyum, M. Malej, M. Y. Lam, F. Shi, C. Angelini, and A. Sheremet, "On the problem of modeling the boat wake climate: The Florida intracoastal waterway," JGR Oceans **126**, e2020JC016676 (2021).
[53]A. G. Samaras and T. V. Karambas, "Numerical simulation of ship-borne waves using a 2DH post-Boussinesq model," Appl. Math. Modell. **89**, 1547–1556 (2021).
[54]M. Malej and F. Shi, "Suppressing the pressure-source instability in modeling deep-draft vessels with low under-keel clearance in FUNWAVE-TVD," Report No. 55 (Engineer Research and Development Center, 2021).
[55]N. J. MacDonald, "Numerical modelling of coupled drawdown and wake," in Proceedings Canadian Coastal Conference (2003).
[56]H. Bihs, A. Kamath, M. Alagan Chella, A. Aggarwal, and O. A. Arntsen, "A new level set numerical wave tank with improved density interpolation for complex wave hydrodynamics," Comput. Fluids **140**, 191–208 (2016).
[57]N. G. Jacobsen, D. R. Fuhrman, and J. Fredsøe, "A wave generation toolbox for the open-source CFD library: OpenFoam®: WAVE GENERATION TOOLBOX," Numer. Methods Fluids **70**, 1073–1088 (2012).
[58]D. Bayraktar Ersan and S. Beji, "Numerical simulation of waves generated by a moving pressure field," Ocean Eng. **59**, 231–239 (2013).
[59]T. H. Havelock, "The propagation of groups of waves in dispersive media, with application to waves on water produced by a travelling disturbance," Proc. R. Soc. London Ser. A **81**, 398–430 (1908).
[60]H. Lamb, *Hydrodynamics*, 6th ed. (Cambridge University Press, 1932).
[61]E. F. Bartholomeusz, "The reflection of long waves at a step," Proc. Campbridge Philos. Soc. **54**, 106–118 (1958).
[62]WSV, see https://www.kuestendaten.de/Tideweser/DE/Service/Kartenthemen/Kartenthemen_node.html for "Wasserstrassen und Schifffahrtsverwaltung des Bundes: Portal Tideweser" (2012).
[63]N. G. Bhowmik, M. Demissie, and S. Osakada, "Waves and drawdown generated by river traffic on the Illinois and Mississippi Rivers," Report No. 271 (Illinois State Water Survey, 1981).
[64]I. Viola, P. Bot, and M. Riotte, "On the uncertainty of CFD in sail aerodynamics," Numer. Methods Fluids **72**, 1146–1164 (2013).